Characterization of electron clouds in the Cornell Electron Storage Ring Test Accelerator using TE-wave transmission

S. De Santis and J.M. Byrd
Lawrence Berkeley Nation Laboratory, Berkeley, California 94720, USA

M. Billing, M. Palmer, and J. Sikora
Cornell University, Ithaca, New York 14853, USA

B. Carlson
Grove City College, Grove City, Pennsylvania 16127, USA

This work was supported by the Director, Office of Science, Office of Fusion Energy Sciences, of the U.S. Department of Energy under Contract No. DE-AC02-05CH11231.

Characterization of electron clouds in the Cornell Electron Storage Ring Test Accelerator using TE-wave transmission

S. De Santis and J. M. Byrd
Lawrence Berkeley National Laboratory, Berkeley, California 94720, USA

M. Billing, M. Palmer, and J. Sikora
Cornell University, Ithaca, New York 14853, USA

B. Carlson
Grove City College, Grove City, Pennsylvania 16127, USA
(Received 17 April 2010; published 15 July 2010)

A relatively new technique for measuring the electron cloud density in storage rings has been developed and successfully demonstrated [S. De Santis, J. M. Byrd, F. Caspers, A. Krasnykh, T. Kroyer, M. T. F. Pivi, and K. G. Sonnad, Phys. Rev. Lett. **100**, 094801 (2008).]. We present the experimental results of a systematic application of this technique at the Cornell Electron Storage Ring Test Accelerator. The technique is based on the phase modulation of the TE mode transmitted in a synchrotron beam pipe caused by the periodic variation of the density of electron plasma. Because of the relatively simple hardware requirements, this method has become increasingly popular and has been since successfully implemented in several machines. While the principles of this technique are straightforward, quantitative derivation of the electron cloud density from the measurement requires consideration of several effects, which we address in detail.

DOI: 10.1103/PhysRevSTAB.13.071002 PACS numbers: 29.20.db

I. INTRODUCTION

The accumulation of low-energy background electrons in the beam pipe of a synchrotron presents a serious limitation on the circulation of high-intensity beams, particularly positively charged beams [1–4]. Primary electrons are created by several mechanisms such as photoemission from synchrotron radiation striking the beam pipe and beam collisions with pipe walls and residual gas. The primary electrons are subsequently accelerated by the electric field of passing beam bunches into the beam pipe, resulting in the production of secondary electrons. A resonant condition can take place between the transit time of background electrons across the beam pipe and the passage of bunches, resulting in a rapid increase in the background electron density, or "electron cloud." External magnetic fields (dipoles, quadrupoles, wigglers) can also concentrate those low-energy electrons in transversally narrow regions of the beam pipe, amplifying the deleterious effect on the circulating beams.

Several approaches have been adopted to mitigate the effects of the electron clouds. One approach is to directly sense any induced motion of the high-energy beam and use active feedback to damp the instabilities created by the electron cloud [5]. Another approach is to directly reduce the growth of the electron clouds by reducing the secondary electron yield of the beam pipe. Characterization and mitigation of the electron cloud effect constitutes one of the main activities in the Cornell Electron Storage Ring Test Accelerator (CesrTA) research program [6]. Several methods have been developed to experimentally study electron clouds such as retarding field analyzers (RFAs) [7–9] and shielded pickups [10] which directly detect background electrons and witness bunches [11]. All of these methods derive the electron density from other measured quantities.

In this paper we present results from CesrTA obtained using the microwave transmission technique [12]. This technique is based on the transmission of a microwave signal in the lowest TE waveguide mode in a section of a synchrotron beam pipe and measuring the phase modulation caused by the periodic variation of the density of the electron plasma. We henceforth refer to this as the TE-wave transmission method. This method offers the advantage of being easily implemented in any sector of an accelerator where beam position monitors (BPMs) are available as antennas for coupling the wave in and out of the vacuum chamber and the analysis of the signal can be done with test equipment readily available in any accelerator laboratory. We also present several subtleties and technical details of the microwave transmission technique.

In Sec. II we describe our measurement technique and its general principles. In Sec. III we discuss its practical implementation and the details of deriving a quantitative measurement of the electron cloud density (ECD) from this

measurement. A selection of measurements made at CesrTA using this technique are presented in Sec. IV and we summarize and conclude in Sec. V.

II. *TE*-WAVE TRANSMISSION MEASUREMENT TECHNIQUE

Figure 1 shows a schematic diagram illustrating the principle of the technique. A traveling electromagnetic wave is excited via antennas and detected with another set of antennas after propagating through a section of the beam pipe with electron cloud. The signal is then analyzed to determine the amplitude of phase modulation, typically using a spectrum analyzer. The presence of the electron cloud changes the phase velocity of the wave, reducing the phase shift per unit propagation length. Analytically, an additional term ω_p^2 is introduced in the expression of the propagation constant for a guided wave given by

$$k_z = \sqrt{\frac{\omega^2 - \omega_{co}^2 - \omega_p^2}{c^2}}, \tag{1}$$

where ω_{co} is the beam pipe cutoff angular frequency of the lowest frequency TE mode and $\omega_p = \sqrt{n_e q_e^2/m_e \varepsilon_0}$ is the plasma angular frequency, which is proportional to the square root of the electron density n_e (q_e is the electron charge, m_e its mass, and ε_0 the permittivity of free space). In the absence of an electron plasma, Eq. (1) reduces to the usual dispersion relation for waveguide propagation. Note that the pipe cutoff frequency is increased by the presence of the electron cloud, although this is a small effect in all practical cases. The plasma angular frequency is given by

$$\omega_p = k_{z0} c \sqrt{1 - \left(1 - \frac{\Delta\varphi}{k_{z0} L}\right)^2}, \tag{2}$$

where $\Delta\varphi$ is the additional phase shift due to the ECD, L is the propagation length, and the mode propagation constant is given by $k_{z0} = \frac{1}{c}\sqrt{\omega^2 - \omega_{co}^2}$. The electron density can be calculated directly from the measured phase shift. For long propagation lengths, or small values of the total phase shift, Eq. (2) can be approximated as

$$\omega_p = c\sqrt{2k_{z0}\Delta\varphi/L}. \tag{3}$$

Ordinary BPM buttons or striplines are used to couple the signal from an external generator into the beam pipe and excite a propagating TE wave (carrier) in the beam pipe. The excitation frequency is chosen to be above the cutoff frequency of the first TE mode and below that of the first high-order mode. The signal is coupled out of the beam pipe some distance further along the accelerator with another set of BPMs. By measuring the phase delay of the wave it is possible to infer the maximum value of the ECD, averaged along that portion of beam pipe.

For typical values of the electron cloud density (10^{11}–10^{12}/m^3), the phase shift over a few meters is on the order of tens of mrad. Static measurement of such small phase delays is not practical in most cases, due to a strong dependence of the absolute value of the phase shift on beam conditions. In this approach, we take advantage of the presence of gaps in the beam fill pattern: during the gap transit between transmitting and receiving point, the ECD decays therefore introducing a phase modulation of the transmitted wave with the gap period. For a single gap this is equal to the ring revolution period. By measuring the modulation depth, one can calculate the maximum phase shift and therefore the ECD.

Although the concept for this technique is simple, deriving an accurate estimate for the ECD requires some understanding of the details of the electron cloud phenomenon and of the electromagnetic environment in a real accelerator. For example, shown in Fig. 2 is a typical measurement of the frequency spectrum of a receiver signal measured in the Cornell Electron Storage Ring (CESR) Test Accelerator. The excited TE wave (carrier) and numerous modulation sidebands generated by the ECD-induced phase shift are interlaced with strong direct beam signals

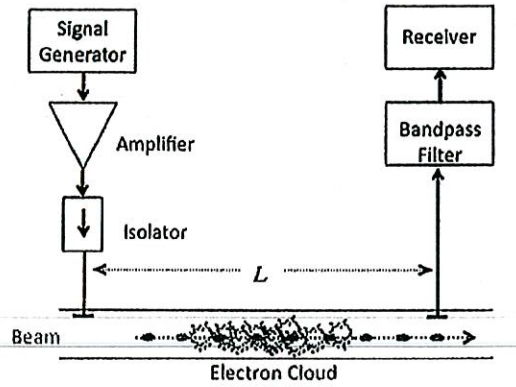

FIG. 1. (Color) Schematic view of the TE-wave transmission technique for measuring the electron cloud density.

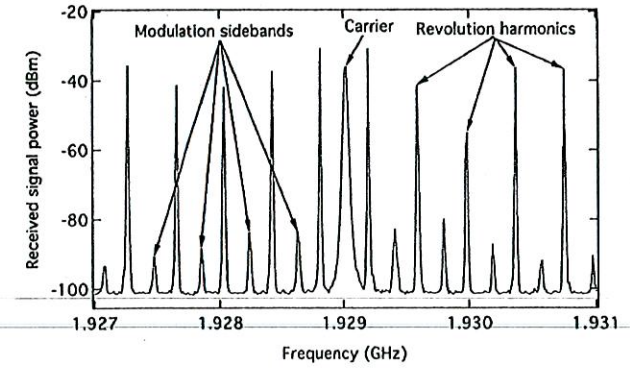

FIG. 2. (Color) Example of phase modulated TE wave and direct beam signal on a CesrTA beam position monitor.

generated by the circulating bunches. The presence of the modulation sidebands is already a good indicator of the presence of electron clouds and a rough estimate can be made on the average electron cloud density between the transmitter and receiver. However, higher accuracy measurements must account for several effects as discussed in detail in the next section.

III. MEASUREMENT PROCEDURE

In this section, we elaborate on four aspects of the measurement procedure: excitation of a single mode (fundamental) propagating in the accelerator beam pipe; detection of the mode after propagation along a certain length of beam pipe; derivation of the phase shift from the observed phase modulation sidebands; and calculation of the average electron cloud density per unit length that would theoretically cause an identical total phase shift.

A. *TE*-wave excitation

The first objective when implementing this method is exciting a *TE* waveguide mode with the largest possible amplitude in the beam pipe. In order to achieve a high resolution in the measurement, the received carrier level should to be as high as possible above the noise level of the signal detector. In an ideal situation, it is straightforward to excite the *TE* mode with dedicated antennas. However, in all of our measurements, we have used existing button-style BPMs as the antennas for coupling the signal in and out of the beam pipe. This can also be seen as an advantage of this method, since it allows measurements all around the ring, wherever standard BPMs are available. Unfortunately typical BPMs are not designed for exciting a *TE* wave, but rather for detecting the fields of a TEM-like wave (i.e. bunch wakefield). Therefore the coupling coefficient to the *TE* wave can be small. An additional difficulty in machines with long bunches is that the BPM and its electronics are designed to operate at frequencies substantially lower than the beam pipe cutoff and their impedance matching above the beam pipe cutoff frequency can be quite poor. Signal generator power cannot be applied indiscriminately, since above certain levels damage of the BPM components can occur. A good standard practice is to use 180° hybrids and combiners and split the power between pairs of opposite buttons, or striplines, in the vacuum chamber, which lowers the power on a single BPM and improves the coupling to the *TE* mode electric field, as illustrated in Fig. 3.

This arrangement also reduces the reverse power towards the generator coming from the direct beam signal, which could induce nonlinearities in the signal generator or the amplifier. This distortion would show as sidebands at the beam revolution frequency in the received signal, which would be indistinguishable from the modulation sidebands due to the electron cloud. Hybrids are also used on the receiving BPM to reject direct beam signal as much as possible.

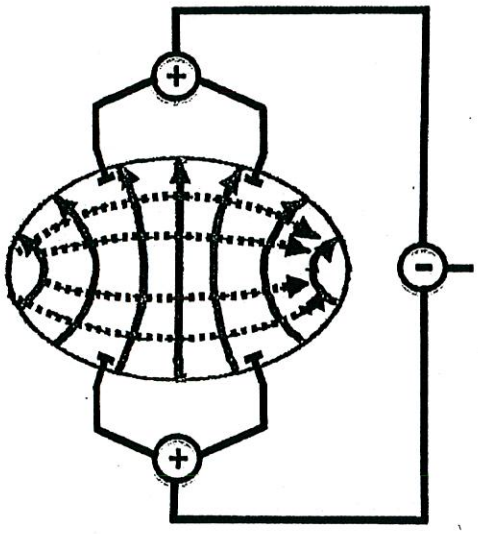

FIG. 3. (Color) BPM optimized for *TE* wave transmission and detection. $TE_{1,1}$ mode field lines are shown.

In selecting the frequency of the excitation, it is clear that the frequency be above the cutoff frequency for the lowest *TE* mode in the beam pipe and be chosen to lie in between beam harmonics as shown in Fig. 2. From Eq. (1) one can easily see that $\Delta\varphi$ is maximized and equal to $\frac{\omega_p}{c}L$ when $\omega = \sqrt{\omega_{co}^2 + \omega_p^2}$. However, many accelerator beam pipes deviate from an ideal waveguide, particularly near cutoff, due to several reasons such as nonuniform cross section, pumping ports, vacuum valves, etc. For example, consider the measured attenuation of the excitation signal in one of the CesrTA configurations shown in Fig. 4. This was measured in one of the beam pipe sections described in Sec. V. The *TE* cutoff is clearly visible just above 1.9 GHz; the transmission deviates from ideal with a minimum near 2.15 GHz. We have found that a good choice for excitation frequency is a few tens of MHz above cutoff, wherever a maximum in transmission can be found.

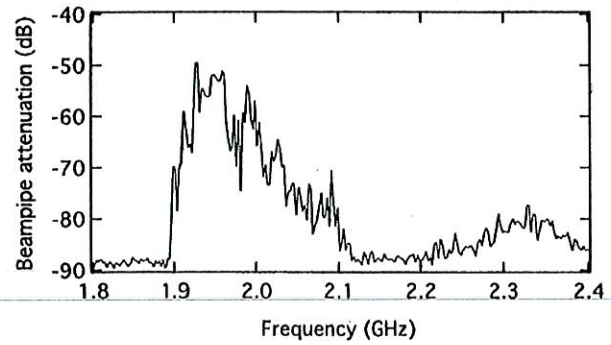

FIG. 4. (Color) Example of measured transmission function for the *TE* wave (CESR dipole).

B. *TE*-wave detection

At the receiver, the maximum sensitivity to ECD occurs with the maximum detection of the transmitted carrier above the noise floor of the detector. In most machines the direct beam signal picked up by the receiving BPM is much stronger than the transmitted signal. As we already stated, this can induce nonlinearities in the receiver and also in the transmitter. The transmitting BPM also couples strongly to the beam, so filters, isolators, and sometimes attenuators have to be used to ensure that the measurement is not affected.

In addition, propagation losses along the beam pipe also contribute to reducing the received signal power. Actual vacuum chamber shapes (bends, antichambers,) and the presence of various components (pumps, rf cavities, etc.) on the pipe can in some instances make the signal detection virtually impossible even for short propagation lengths [13]. Reducing the distance between BPMs by choosing sets closer to each other can be used as a remedy, although this increases the number of measurements necessary for measuring a given length of beam pipe.

In Eq. (3) it is assumed that the electron cloud modulates only the phase of the transmitted signal. The theory of propagation of electromagnetic waves in a cold electron plasma only points to a phase delay effect [14]. Yet, recent measurements [15] have evidenced also an attenuation effect in the presence of magnetic fields, which results in an amplitude modulation (AM) component. Possible causes are electrons in the ECD having a nonzero energy spread, or by resonant interaction with external magnetic fields. It is also possible that variation with frequency of the transmission of the beam pipe can lead to conversion of phase modulation to amplitude modulation. In any case, the AM component in the measured sidebands needs to be recognized as such and separated from the PM component, which is the one to be used in the calculation of the ECD.

Unfortunately, AM and PM sidebands cannot be separated by a simple amplitude measurement in all practical cases. At low modulation index (small phase shifts and small attenuations) AM and PM sidebands look identical. If a vector spectrum analyzer is available, then the two modulations are phase shifted by 90° as the following calculations show: For example, we can write a generic signal with amplitude and phase modulation in the form

$$s(t) = [1 - m_{\mathrm{AM}}(t)]\cos[\omega_c t + m_{\mathrm{PM}}(t)], \tag{4}$$

where ω_c is the carrier angular frequency and m_{AM} and m_{PM} are the modulating functions. In the hypothesis of low modulation indexes (which is generally the case encountered in practice) $|m_{\mathrm{AM}}(t)| \ll 1$ and $|m_{\mathrm{PM}}(t)| \ll 1$ and Eq. (4) can be approximated as

$$\begin{aligned} s(t) &\approx [1 - m_{\mathrm{AM}}]\left\{\cos(\omega_c t)\left[1 - \frac{m_{\mathrm{PM}}^2}{2}\right] - \sin(\omega_c t) m_{\mathrm{PM}}\right\} \\ &\approx \cos(\omega_c t) - m_{\mathrm{AM}}\cos(\omega_c t) - m_{\mathrm{PM}}\sin(\omega_c t) + \cdots. \end{aligned} \tag{5}$$

The time dependence of the modulating functions has been omitted for the sake of brevity. The Fourier transform of the rightmost term in Eq. (5) is

$$\begin{aligned} S(\omega) = &\frac{1}{2}[\delta(\omega + \omega_c) + \delta(\omega - \omega_c)] \\ &- \frac{1}{2}[M_{\mathrm{AM}}(\omega + \omega_c) + M_{\mathrm{AM}}(\omega - \omega_c)] \\ &- \frac{i}{2}[M_{\mathrm{PM}}(\omega + \omega_c) - M_{\mathrm{PM}}(\omega - \omega_c)], \end{aligned} \tag{6}$$

where δ is a Dirac delta function and M_{AM} and M_{PM} are the transforms of the modulating functions. The three terms on the right-hand side of Eq. (6) respectively originate the carrier, AM sidebands, and PM sidebands that one would observe in an actual measurement. Comparing the expressions for the AM and PM sidebands, it is evident that both transforms $M_{\mathrm{AM}}(\omega)$ and $M_{\mathrm{PM}}(\omega)$ have an even real part and an odd imaginary part. Furthermore, due to their periodicity, both functions consist in a series of pulses separated by the ring revolution frequency f_{rev}. When we operate an amplitude measurement of the sidebands, the total measured signal, omitting the obvious carrier related term, is given by

$$\begin{aligned} |S(\omega)| = &\{[\mathrm{Re}(M_{\mathrm{AM}}) - \mathrm{Im}(M_{\mathrm{PM}})]^2 \\ &+ [\mathrm{Im}(M_{\mathrm{AM}}) + \mathrm{Re}(M_{\mathrm{PM}})]^2\}^{1/2} \\ = &\{|M_{\mathrm{AM}}|^2 + |M_{\mathrm{PM}}|^2 + 2[\mathrm{Im}(M_{\mathrm{AM}})\,\mathrm{Re}(M_{\mathrm{PM}}) \\ &- \mathrm{Re}(M_{\mathrm{AM}})\,\mathrm{Im}(M_{\mathrm{PM}})]\}^{1/2}. \end{aligned} \tag{7}$$

From Eq. (7) we can see that a measurement of the modulated signal amplitude will generally yield upper and lower sidebands of different amplitudes, whereas, when only one type of modulation is present, the sidebands will be symmetric. From the point of view of the phase shift determination, we need to exclude the part of the modulated signal due to amplitude modulation. While the observation of asymmetric sidebands tells us that both modulations are present, we cannot tell whether the AM or the PM component is dominant. Therefore, even slightly asymmetric sidebands do not guarantee that the AM component is negligible. These considerations point to the necessity of an accurate theoretical study of the attenuation in the wave propagation through an electron cloud filled region.

On a final note, the method described in this paper averages variations of the ECD along the *TE* wave path. If a more local measurement is required, one can always use nearby BPMs, with the stipulation that their distance has to be large compared to the decay lengths of the higher order modes, which are short anyway. Although formulas

suggest that using short beam pipe lengths would only originate a proportionally lower phase shift, which is harder to measure, this is more than compensated by the reduction in the propagation attenuation.

C. Phase shift calculation

A number of effects can affect the phase delay estimate from the modulation sidebands height: the sidebands only depend on changes of the phase delay and not on its absolute value; reflections and standing waves can modify the effective propagation length of the *TE* wave; the sidebands also depend on how the ECD changes in time and not only on how much.

1. Effect of the gap length

Another possible source of error in the calculation of the ECD from phase shift measurement results from the fact that the method is intrinsically only sensitive to relative changes of the phase shift, or that is to say to the modulation depth. It can be easily recognized that, in the event of a persistent ECD that is not able to be cleared by a short gap in the bunch train, our measurements would underestimate the maximum value of the ECD, since it would not measure that portion of constant ECD level continuously present in the machine. An easy solution for this problem, if one can select the fill structure, is to take measurements at different gap lengths, while maintaining the total circulating current constant. No sidebands should be visible with no gap, or a very short one, and as the gap length is increased one should measure an increase in the sidebands up to the point where the gap is long enough to entirely clear the accumulated ECD at its passage, since the electron creation mechanism is proportional to the total beam current in first approximation. If possible this measurement should be performed with an electron beam, where the secondary emission phenomena, which are more sensitive to the actual beam distribution, are usually strongly reduced. Experimental results show that in CesrTA a gap from 100 to 200 ns long, depending on the particular location, is amply sufficient to clear any ECD.

2. Effect of TE wave reflections

A further complication lays in the value to use for the propagation distance L. In its simple formulation the method assumes that the *TE* wave is traveling only from the transmitting (Tx) BPM to the receiving (Rx) BPM and L is simply equal to the geometrical distance between Tx and Rx. In reality, the Tx BPM will excite waves traveling in both directions along the beam pipe and the wave continues to propagate after reaching the Rx BPM. If the machine is long enough that the *TE* wave cannot travel all around its circumference before being completely attenuated, this is not a problem, since the wave effectively samples only once the beam pipe region between the two BPMs. Reflections from discontinuities upstream or downstream of the buttons can change the effective propagation distance. For example, reflections of the *TE* wave traveling past the Rx BPM would contribute to the total phase shift adding an extra portion of beam pipe, with its particular ECD, that contributes to the total phase shift.

3. Effect of the ECD rise/fall time

Figure 5 qualitatively shows phase shift as a function of time in a case where the bunch train is long enough to reach a steady state in the ECD, the bunch spacing is much shorter than the ECD rise/fall time, and the gap length is sufficient to reduce the ECD to zero. In general, due to the periodic nature of the ECD in a synchrotron ring, the modulation spectrum appears composed of lines spaced at the revolution frequency f_{rev} around the *TE* wave frequency. Obviously, in the case of N identical trains, equally spaced, the modulation spectrum lines will be spaced at $N \times f_{rev}$. Such a spectrum contains all the information about time evolution and amplitude of the ECD-induced phase shift. In principle, one could simply demodulate the modulation spectrum and reconstruct $\Delta\varphi$ as a function of time. The presence of a direct beam signal makes this not a simple procedure since one needs to filter it out across the entire frequency span where sidebands are measured. Where the beam signal level is substantially lower than the modulation sidebands, this can be easily achieved by attenuators [16], but this is a rare event. For most machines, sidebands are well below beam harmonics and sophisticated filters would have to be used. To obtain an estimate of the phase shift approximations can be introduced, especially when one is only interested in its maximum value and the time scale of its variations, which is directly linked to the ECD rise and fall times. Previous works [12,17] have assumed a simple sinusoidal phase modulation, which would only generate an upper and a lower sideband for small modulation indexes. In that case the estimate of the

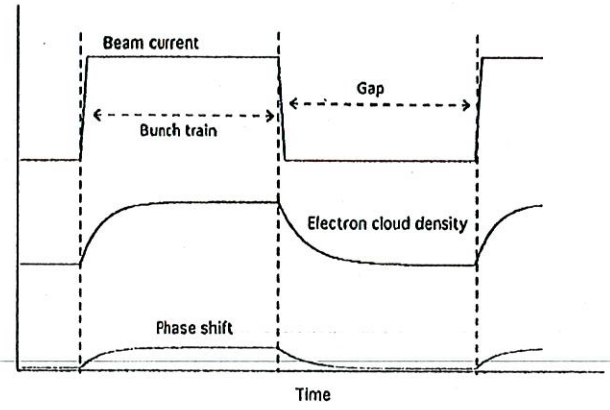

FIG. 5. (Color) Qualitative time evolution of beam current (red), electron cloud density (blue), and phase shift (green).

maximum ECD only depends on the sidebands amplitude relative to the carrier SB_c and the relative phase shift is simply

$$\Delta\varphi = 2SB_c. \tag{8}$$

In practical cases, one usually observes a number of sidebands, even for small modulation depths, as shown in Fig. 2. A better approximation can be obtained assuming that rise and fall times of the ECD are much shorter than the bunch train length, but still at least comparable with the bunch spacing. In such a case, which is often verified, a rectangular modulating function, with duty factor equal to the train length divided by the machine length, can obviously be seen as a more accurate representation than a sinusoidal one. This hypothesis can find a degree of experimental verification by looking at the sidebands with different train lengths. Figure 6 shows a detail of measurements in a dipole region of CesrTA with bunch trains of different lengths equal to one-fourth, one-fifth, and one-sixth of the ring circumference. One can see that correspondingly every fourth, fifth, and sixth beam harmonic is suppressed. The general properties of the Fourier transform point out how this behavior is evidence of a strong rectangular modulation component. In such a case we can modify Eq. (8), by introducing a correction factor that takes into account the rectangular nature of the modulation and we have

$$\Delta\varphi = \frac{1}{2}SB_c\frac{\pi}{\sin(\pi t_b f_{\text{rev}})}, \tag{9}$$

where t_b is the bunch train length. Applying the *Carson's bandwidth rule* [18], an approximate evaluation of the ECD rise and fall times (t_r) is given by

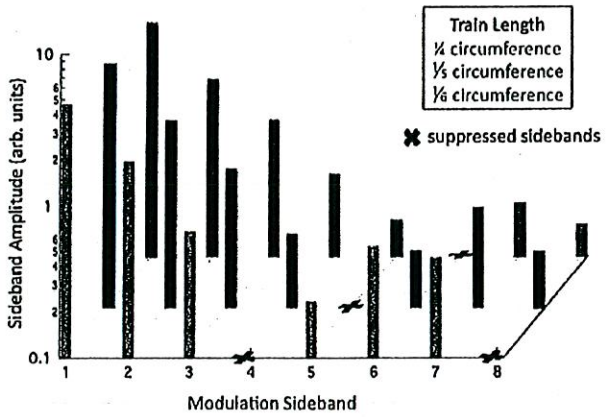

FIG. 6. (Color) Cancellation of modulation sidebands due to different bunch train lengths. Suppressed modulation sidebands due to the rectangular modulation function are indicated for various train lengths.

$$t_r \approx \frac{2}{3}\frac{1}{f_{\text{rev}}N_{\text{SB}}}, \tag{10}$$

where N_{SB} is the number of visible sidebands.

D. Electron cloud density estimate

Once the additional phase shift is known, one has to keep in mind that Eq. (1) was derived for uniformly distributed plasma and for electrons of very low, or zero, energy (cold plasma). Additionally, absorption is not taken into account, which would result in a AM term. This can be a strong effect in the presence of magnetic fields, when particular conditions of resonance between *TE* wave and magnetic field are verified.

1. Transverse distribution of the ECD

In Sec. II, we assumed that the transverse distribution of the ECD was uniform. However, it has been shown [19] that the presence of magnetic fields can result in distinct transverse distributions. For example, in vertical dipole fields the ECD can be concentrated in vertical stripes near the pipe center. A detailed analysis of this effect is beyond the scope of this paper. For the purposes of our present analysis, we assume that the overall measured phase shift represents an average over the ECD. The transverse average is furthermore weighted by the *TE* field transverse shape so that, given the fundamental mode field distribution, it is reasonable to expect that the ECD near the beam pipe center originates a larger phase shift than the ECD near the pipe walls, although they may have the very same average transverse density. Although this effect has some benign characteristics, since it overestimates the ECD in those cases where it affects the circulating beam to a larger degree, substantial efforts are currently underway to be able to quantify this effect with computer simulations and experimental measurements.

2. Effect of ECD temperature

Besides potentially introducing an AM component, a nonzero temperature electron plasma (warm plasma) can also change the value of the PM component. The following calculations show how in practical cases this change is small and can usually be neglected. The expression for the plasma angular frequency $\omega_p = \sqrt{n_e q_e^2/m_e\varepsilon_0}$ is valid only for a cold plasma. For a warm plasma, characterized by a thermal velocity of the electrons v_{th}, we can define a wavelength-dependent angular frequency for the warm plasma

$$\omega_{pw}^2 = \omega_p^2 + 3k^2v_{\text{th}}^2, \tag{11}$$

where k is the wave number. By replacing ω_{pw} in the dispersion relation [Eq. (1)], we obtain for the propagation constant

$$k_z^2 = \frac{\omega^2}{c^2}(1 - 3v_{th}^2/c^2) - \frac{\omega_{co}^2}{c^2} - \frac{\omega_p^2}{c^2}. \quad (12)$$

We see that the only difference with the cold plasma case is in the thermal velocity dependent term. By designating $\hat{\omega} = \omega\sqrt{1 - 3v_{th}^2/c^2} < \omega$, we can write the approximated expression for the phase shift per unit length like

$$\frac{\Delta\varphi}{L} \approx \frac{\omega_p^2}{2c\sqrt{\hat{\omega}^2 - \omega_{co}^2}} \quad (13)$$

which indicates that a warm electron plasma will generate a larger phase shift in a propagating EM wave than a corresponding cold plasma with the same density. Yet, even a thermal velocity equal to one-tenth of the speed of light (2.5 keV) would only account for a difference of a few percent with the cold plasma case.

IV. RESULTS AT CESRTA

One of the principal goals of CesrTA is to advance the International Linear Collider R&D program into mitigation measures that can reduce the ECD buildup to levels which will maximize the safety margin for stable positron damping ring operation. Support for EC experimental areas and instrumentation upgrades to aid in beam dynamics studies and low emittance tuning are central components of the CesrTA program. This includes deployment of local EC diagnostics in vacuum chambers in each of the representative magnetic field regions in CESR. General parameters of CesrTA are shown in Table I.

The *TE* wave method analyzed in the previous sections is currently used in several locations of the CESR ring (Fig. 7) to measure the evolution of the electron cloud with different beam conditions and test the effectiveness of various mitigation techniques such as vacuum chamber geometry and coating, clearing solenoids, and clearing electrodes. The L3 region includes a circular beam pipe, half of which is equipped with a clearing solenoid, while the other half includes a chicane with four dipoles, each with a different vacuum chambers: aluminum, grooved, carbon coated, and TiN coated. The L0 region comprises six superconducting wigglers on a straight beam pipe. The dipole and wiggler replacement chamber (WRC) region is equipped with a 1.1 T dipole and a section of straight beam

TABLE I. CesrTA parameters.

Energy	2, 4, or 5 GeV
Circumference	768 m
rf frequency	500 MHz
Harmonic number	1281
Bunch spacing	4,8,12, or 14 ns
Number of bunches	1 to 122
Bunch charge	Up to 4 mA
Bunch length	30 to 52 ps

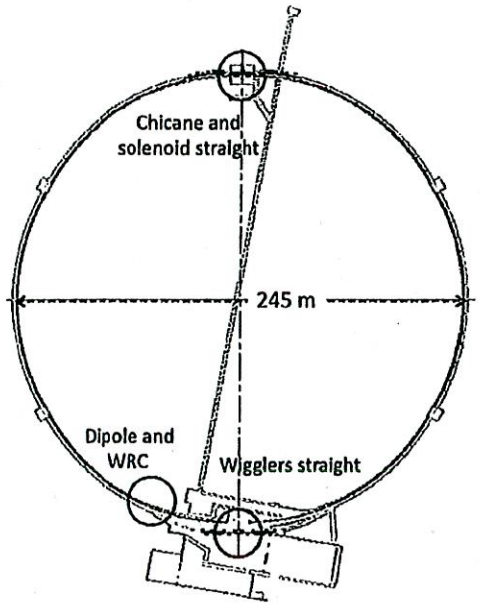

FIG. 7. (Color) The *TE* wave measurement is installed in three locations in the CESR ring.

pipe. In all cases we applied the considerations described in previous sections: measured the relative height of the first sidebands; compensated for variation in the transfer function at the respective frequencies; applied the correction factor for rectangular modulation; and calculated the modulation depth.

An example of sideband measurement in the wiggler straight is shown in Fig. 8, where we are measuring the sidebands generated by a 45-bunch positron train of 60 mA total current in a *TE* wave traveling along the eastern half of the L0 wiggler straight. The relative amplitude of upper and lower sidebands (USB and LSB, respectively) have to be corrected for the difference in transmission function of

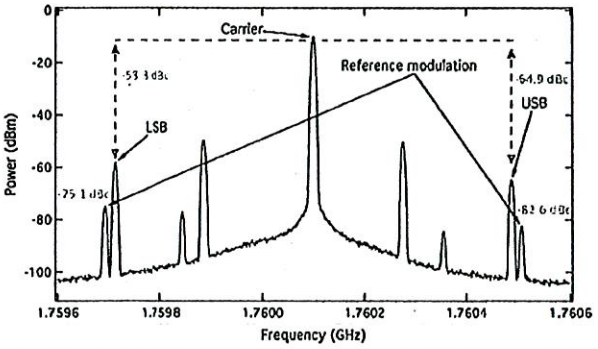

FIG. 8. (Color) Example of sidebands measurement in the wiggler straight: 45-bunch positron train of 60 mA total beam current with 14 ns bunch spacing, with reference modulation sidebands (1 mrad modulation depth at 410 kHz).

the measuring system at the carrier and USB and LSB frequencies. This can be done with separate measurements, but we have recently introduced a calibration phase modulation of known index at a frequency close to the e-cloud modulation frequency, so that the transmission function is about equal to that for the nearby modulation sidebands. In this case the reference phase modulation index at 410 kHz was chosen to be 1 mrad, which should generate sidebands at -66 dBc. We observe lower values from which it is possible to infer the attenuation, with respect to the carrier frequency, at the USB and LSB frequencies (390 kHz). We calculate a correction factor equal to $-66.0-(-64.9)=-1.1$ dB for the LSB and, analogously, $+6.4$ dB for the USB. The corrected value for the LSB is -49.2 and -48.3 dBc for the USB. It is worth noticing that, while before correction the two sidebands were rather different (6.6 dB), after the correction is applied their values are almost identical, as expected. The small residual difference of less than 1 dB can be attributed to experimental errors and noise sources described previously.

Being able to continuously monitor the transmission function at the frequencies of interest is quite important during some experiments when beam and/or machine conditions undergo large variations. In such cases, the transmission changes due mostly to thermal effects can disrupt the measurement as shown in Fig. 9: While ramping the wigglers magnetic field, the emitted synchrotron radiation increase can change the beam pipe transmission function at the sidebands frequency so that USB and LSB amplitudes actually appear to diverge during the experiment until correction is applied.

To estimate the ECD from the sidebands measured in Fig. 8, we can use the average of the two sidebands -48.8 dBc. A further correction has to be applied to this value: Since separate measurements have shown that the ECD decay time is short compared to the train length used, the phase modulation induced by the ECD is a rectangular rather than a sinusoidal one. For such a modulation the first sideband amplitude is given by Eq. (9). In this case the train was 630 ns long and the phase shift is therefore equal to 8 mrad. Knowing that the propagation length is about 8.7 m, the carrier frequency 1.761 GHz, and the pipe cutoff 1.757 GHz, we can apply Eq. (2) and estimate the ECD as $1.3\times10^{11}\ e^-/\mathrm{m}^3$.

A special feature of the CesrTA ring is the availability of both electron and positron beams, which circulate in opposite directions. We have performed measurements with both beams in order to separate the contribution of primary photoelectrons to the total ECD. Figure 10 shows the difference in the measured ECD generated by a 45-bunch train of electrons or positrons (14 ns bunch spacing), as a function of total beam current. The difference between the two curves is essentially due to the different amount of secondary electrons generated by an electron and a positron beam. It can be seen that, as expected, a positron beam can accelerate low-energy electrons across the beam pipe and extract new electrons from the wall much more efficiently. The overall high levels of electron cloud shown in Fig. 10 are due to the aluminum vacuum chamber.

Another example is given by Fig. 11. With a constant beam of 45×1 mA positron bunches the wigglers are

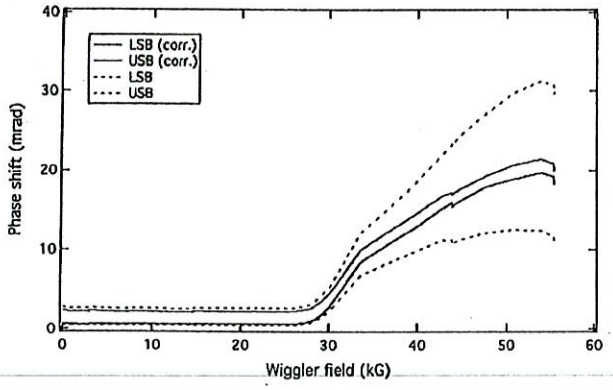

FIG. 9. (Color) Sidebands level relative to the carrier during wiggler ramp in the L0 straight with (solid lines) and without (dashed) correction applied.

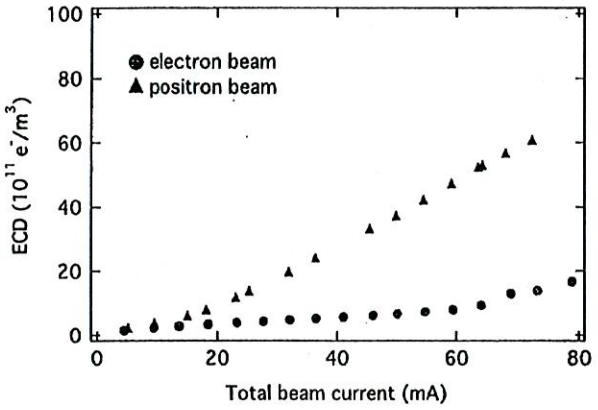

FIG. 10. (Color) Transmission measurements in the dipole region: 45-bunch train positron (blue) and electron (red) beam.

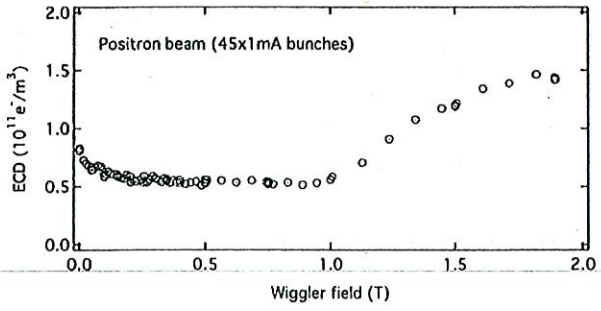

FIG. 11. (Color) Electron cloud density as a function of the wiggler field.

slowly ramped from 0 to 1.9 T, while the sidebands amplitude is measured. The change in electron cloud density with a constant beam, which was simultaneously measured on the RFAs, is due to changes in the synchrotron radiation fan as the wiggler field is ramped.

V. DISCUSSION AND CONCLUSIONS

Microwave transmission has been established as a relatively simple method for experimental measurement of the ECD. This technique can be easily implemented on most storage rings and synchrotrons and, in principle, allows one to monitor any portion of a ring with little more than signal cables and basic rf equipment. However, a quantitative measure of the electron cloud density requires consideration of the time dependence of the modulation by the ECD which depends on details of the bunch fill pattern, although in many cases it is possible to reach a reasonable accuracy by considering only the sidebands next to the carrier. Qualitative measurements are quite straightforward and give excellent measure of the relative ECD for similar bunch fill patterns.

For the case of a nonmagnetized plasma, the electron cloud density can be determined with high accuracy, limited by the AM/PM conversion of the transmitted signal. The presence of magnetic fields can make the transverse distribution of the ECD highly nonuniform, which introduces a further approximation in using a method that instead assumes a uniform distribution. In any case, the *TE* wave has a field with maximum intensity in the center of the pipe and therefore the phase shift depends more strongly on the actual electron distribution in that region. The fact that a heavier weight is given to the region where the bunches are actually passing through can also be seen as a measurement of an effective ECD, the average so estimated being closer to the density seen by the beam, rather than to a purely mathematical average.

[1] K. Ohmi, Phys. Rev. Lett. **75**, 1526 (1995).

[2] K. Ohmi and F. Zimmermann, Phys. Rev. Lett. **85**, 3821 (2000).

[3] R. Cimino, I.R. Collins, M.A. Furman, M. Pivi, F. Ruggiero, G. Rumolo, and F. Zimmermann, Phys. Rev. Lett. **93**, 014801 (2004).

[4] M. Izawa, Y. Sato, and T. Toyomasu, Phys. Rev. Lett. **74**, 5044 (1995).

[5] G. Rumolo, G. Arduini, E. Metral, E. Shapochnikova, E. Benedetto, G. Papotti, R. Galaga, and B. Salvant, Report No. CERN-2008-005, 2008.

[6] M. Palmer *et al.*, in *Proceedings of the 23rd Particle Accelerator Conference, Vancouver, Canada, 2009* (IEEE, Piscataway, NJ, 2009).

[7] R.A. Rosenberg and K.C. Harkay, Nucl. Instrum. Methods Phys. Res., Sect. A **453**, 507 (2000).

[8] K.I. Kanazawa, H. Fukuma, H. Hisamatsu, and Y. Suetsugu, in *Proceedings of the 21st Particle Accelerator Conference, Knoxville, 2005* (IEEE, Piscataway, NJ, 2005), p. 1054.

[9] M. Kireeff Covo *et al.*, Phys. Rev. Lett. **97**, 054801 (2006).

[10] E. Mahner, T. Kroyer, and F. Caspers, Phys. Rev. ST Accel. Beams **11**, 094401 (2008).

[11] W. Fischer, J.M. Brennan, M. Blaskiewicz, and T. Satogata, Phys. Rev. ST Accel. Beams **5**, 124401 (2002).

[12] S. De Santis, J.M. Byrd, F. Caspers, A. Krasnykh, T. Kroyer, M.T.F. Pivi, and K.G. Sonnad, Phys. Rev. Lett. **100**, 094801 (2008).

[13] J. Byrd and T. Kroyer (private communication).

[14] N.A. Krall and A.W. Trivelpiece, *Principles of Plasma Physics* (San Francisco Press, San Francisco, 1986).

[15] T. Kroyer, F. Caspers, and E. Mahner, Proceedings of the 21st Particle Accelerator Conference, Knoxville, 2005 (Ref. [8]), pp. 2212–2214.

[16] N. Eddy, J.L. Crisp, I. Kourbanis, K. Seiya, R.M. Zwaska, and S. De Santis, Proceedings of the 23rd Particle Accelerator Conference, Vancouver, Canada, 2009 (Ref. [6]).

[17] F. Caspers, W. Höfle, J.M. Jiménez, J.F. Malo, J. Tuckmantel, and T. Kroyer, in Proceedings of the 31st ICFA Beam Dynamics Workshop: Electron Cloud Effects (ECLOUD04), Napa, California, 2004 (CERN Report No. CERN-2005-001).

[18] J.R. Carson, Proc. IRE **10**, 57 (1922).

[19] C.M. Celata, M.A. Furman, J.-L. Vay, D.P. Grote, J.S.T. Ng, M.T.F. Pivi, and L. Wang, in Proceedings of the 23rd Particle Accelerator Conference, Vancouver, Canada, 2009 (Ref. [6]).